Int. J. Electrochem. Sci., 9 **(2014)** 2090 - 2100

International Journal of
ELECTROCHEMICAL
SCIENCE
www.electrochemsci.org

Investigation of the Surface Potential on Iron Nanoparticles During the Corrosion by Atomic Force Microscopy (AFM) and Kelvin Probe Force Microscopy (KFM)

X. Joseph Raj and T. Nishimura[*]

Materials Recycling Design Group, Research Center for Strategic Materials, National Institute for Materials Science, Tsukuba, Japan
[*]E-mail: NISHIMURA.Toshiyasu@nims.go.jp

Received: 21 November 2013 / *Accepted:* 17 December 2013 / *Published:* 2 February 2014

The combination of atomic force microscopy (AFM) and Kelvin probe force microscopy (KFM) was a powerful technique to obtain high-resolution maps of the surface potential distribution on the pure iron (Fe) and Stainless steel (SUS:18Cr-8Ni-Fe) nanoparticles. The corrosion behavior of the individual nanoparticle was monitored in 0.1M H_2SO_4 solution with different time. The size and the surface potential of the pure Fe nanoparticles decreased with time in an acid solution, indicating the corrosion of nanoparticles. Similarly, the surface potential of the nanoparticles by KFM decreased with increase in the concentration of the acid. The changes in KFM maps of nanoparticles showed the corrosion corresponded to the anodic reaction by surface potential. The corrosion at pure-Fe surface occurred more severely than that of SUS nanoparticle. Moreover, the decrease of the surface potential of Fe nanoparticle was sharper than SUS nanoparticle. This was due to the keeping of passive film of SUS nanoparticle in severe solution. Therefore, the corrosion of SUS nanoparticle was suppressed by the formation of protective film on the surface. It was concluded that SUS nanoparticle exhibited excellent corrosion resistance compared to Fe nanoparticle in a 0.1M H_2SO_4 solution.

Keywords: AFM, KFM, Nanoparticles, Corrosion, Passivation

1. INTRODUCTION

Nanoparticles have unique optical, electronic, and structural properties that are not available in bulk solids. Thus, nanoparticles play an important role in a wide variety of fields including advanced materials, pharmaceuticals, and environmental detection and monitoring, catalysis [1], biological applications [2] and information storage [3]. For example, iron nanoparticles are being used to clean up carbon tetrachloride pollution in ground water. Besides, iron oxide nanoparticles are being used to

clean arsenic from water wells. Titanium oxide (TiO_2) nanoparticles are used in pigments, gas and humidity sensors, dielectric ceramics, support of catalysis, solar cells [4-6] and other applications.

In recent years, AFM offers both qualitative and quantitative information on many physical properties including size, morphology, surface texture and roughness. A wide range of particle sizes can be characterized in the same scan, from 1 nanometer to 10 micrometers. In addition, the AFM can characterize nanoparticles in multiple mediums including ambient air, controlled environments, and even liquid dispersions. The AFM can distinguish between different materials, providing spatial distribution information on composite materials with otherwise uninformative topographies. Statistics on groups of particles can also be measured through image analysis and data processing. With knowledge of the material density, mass distribution can be easily calculated [7, 8].

KFM has an imaging technique that obtains the variation of the potential between the tip and the sample at each in-plane position. The combination of AFM and KFM is a powerful tool to obtain high-resolution maps of the surface potential distribution on conducting and nonconducting samples. KFM was introduced as a tool to measure the local potential difference between a conducting AFM tip and the sample, thereby mapping the work function or surface potential of the sample with high spatial resolution. KFM has been used in a variety of studies to investigate the electronic properties of chalcopyrite solar cell materials [9]. KFM measures the surface potential with fine spatial resolution of few nm and voltage resolution of (~10 mV) by probing the Coulomb force between AFM tip and sample. KFM has also been used to study the electrical properties of organic materials/devices [10] and biological materials [11, 12]. Recent reports show that KFM can be used to image potential distributions on the surface with sub-nanometer resolution, making KFM the best technique, at present, for characterizing the electrical properties of nanostructures. In corrosion studies, the KFM has been used by a few authors [13–17] for potential measurements. Since the magnitude of the measured electric potential critically depends on the size of the feature, its surroundings, and the probe geometry, a clear understanding of the contrast transfer mechanism in KFM is required to enable a quantitative analysis and interpretation of potential images. The knowledge of the contrast transfer mechanism will permit the combination of high-resolution surface topography and electric potential data which is likely to significantly facilitate the improved characterization of corrosion analysis.

In this work, we investigate the surface topography and surface potential of pure iron and stainless steel nanoparticles (mass %:18 Cr-8 Ni-Fe) in 0.1 M H_2SO_4 by AFM and KFM. The particles were also evaluated using different concentration of an acid and chloride. The size and surface potential of the nanoparticles were analyzed with different processing time in the electrolytes.

2. EXPERIMENTAL

The average size of pure iron and stainless steel nanoparticles was 1300 ± 200 nm and 1200 ± 200 nm, respectively. The nanoparticles were dispersed and stirred for 2 h in ethanol containing 0.1 M H_2SO_4. The surface morphology of the nanoparticles was evaluated by AFM. The AFM observation was performed with a 20 μm scanner in tapping mode and these were conducted three times on different sample to ensure the validity of the data. A modulation bias voltage (25 kHz, 1 V) was

applied between the probe and the sample during KFM measurements. AFM operation during the KFM imaging process was conducted in amplitude detection mode using the noncontact mode.

The KFM technique uses the standard noncontact AFM setup, but the sample is scanned with Pt-coated Si tips with a 20 nm nominal radius. An AC signal is fed 10-20 kHz below the frequency of the normal AFM oscillator, which matches the natural frequency of mechanical oscillation of the cantilever-tip system (40-70 kHz). The image is built using the DC voltage fed to the tip, at every pixel, thus detecting electric potential gradients throughout the scanned area.

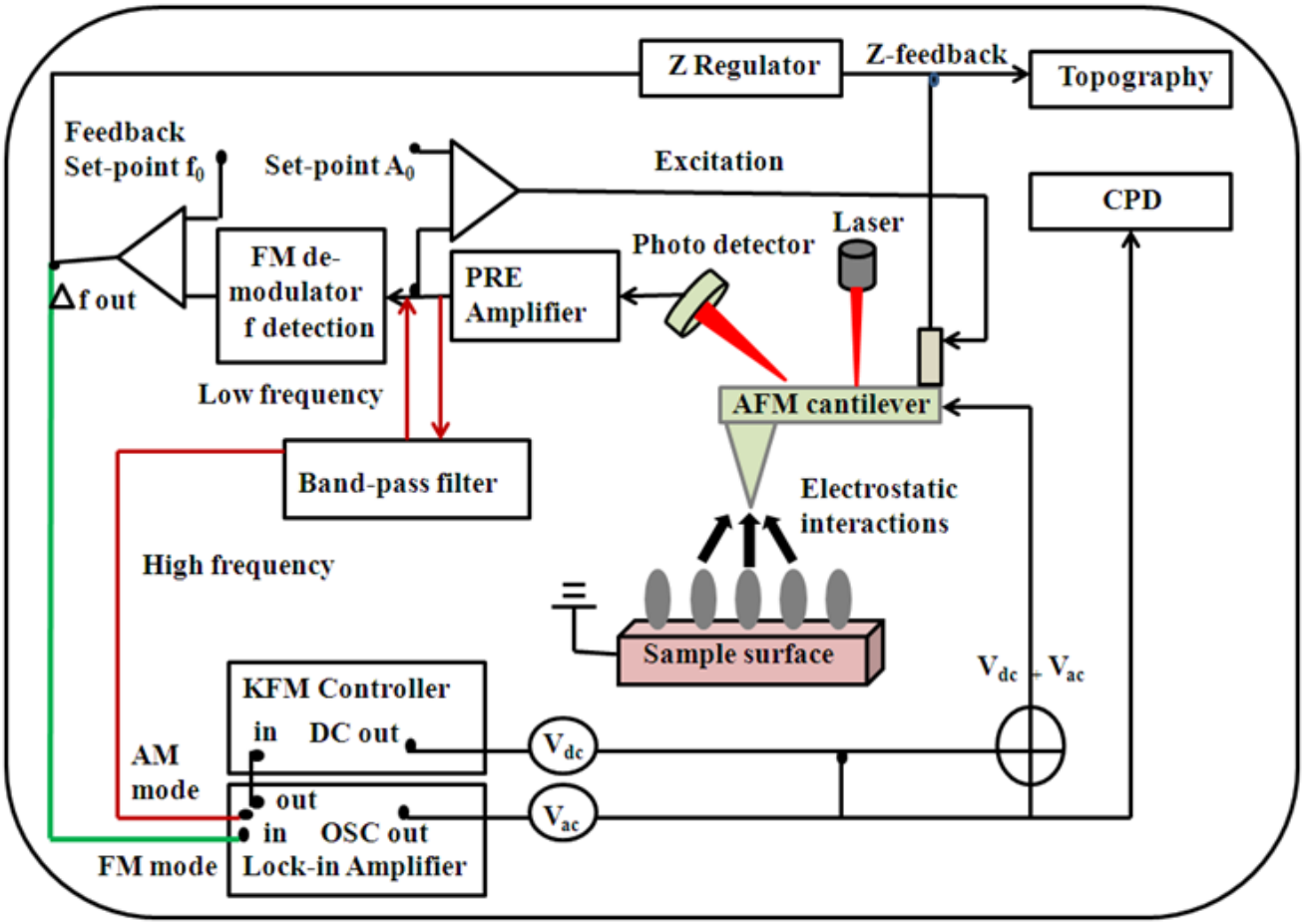

Figure 1. Schematic diagram of AFM and KFM system

Figure 1 shows the schematic diagram of AFM and KFM experimental apparatus. The lower part shows the Frequency Modulation (FM) mode of AFM system for topography measurement and the upper part shows the components for surface potential mapping including the KFM controller and lock-in amplifier. A band-pass filter filters the low and high frequency signals. The low frequency signal is used for topography regulation. The high frequency signal feeds directly into the lock-in amplifier.

3. RESULTS AND DISCUSSION:

3.1. Effect of treatment period on pure iron nanoparticles in 0.1 M H_2SO_4:

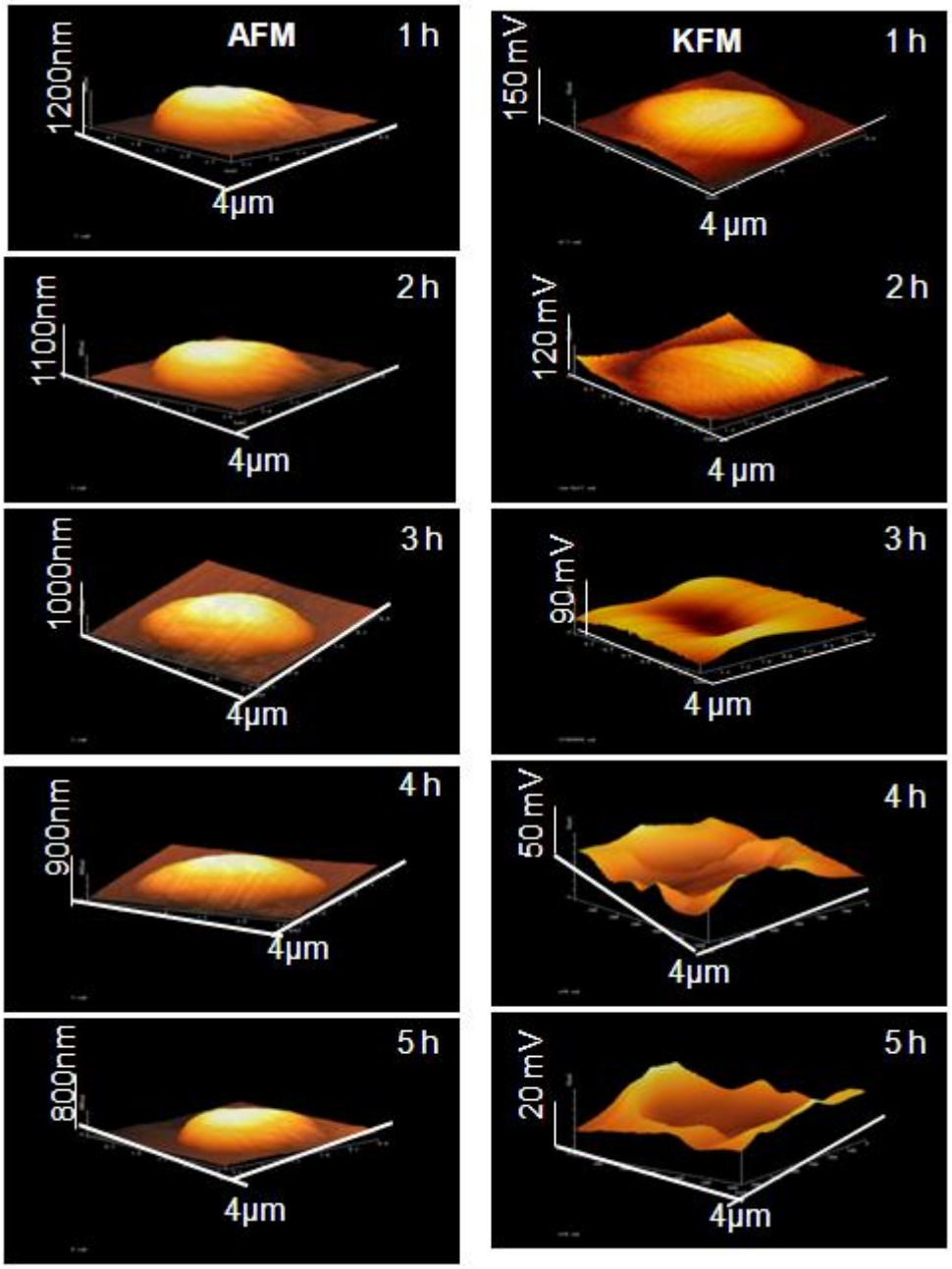

Figure 2. AFM (left) and KFM (right) images of iron nanoparticle treated in 0.1M H_2SO_4 at different hours.

Corrosion behavior of a nanoparticle was described by the electrochemical surface potential. This potential normally means the average value on the whole surface of a specimen. In many cases, however, the surface is divided into anodic and cathodic regions, and hence the local potential is not uniform. Therefore, it is important to know the local potentials using AFM and KFM in order to understand the corrosion phenomena.

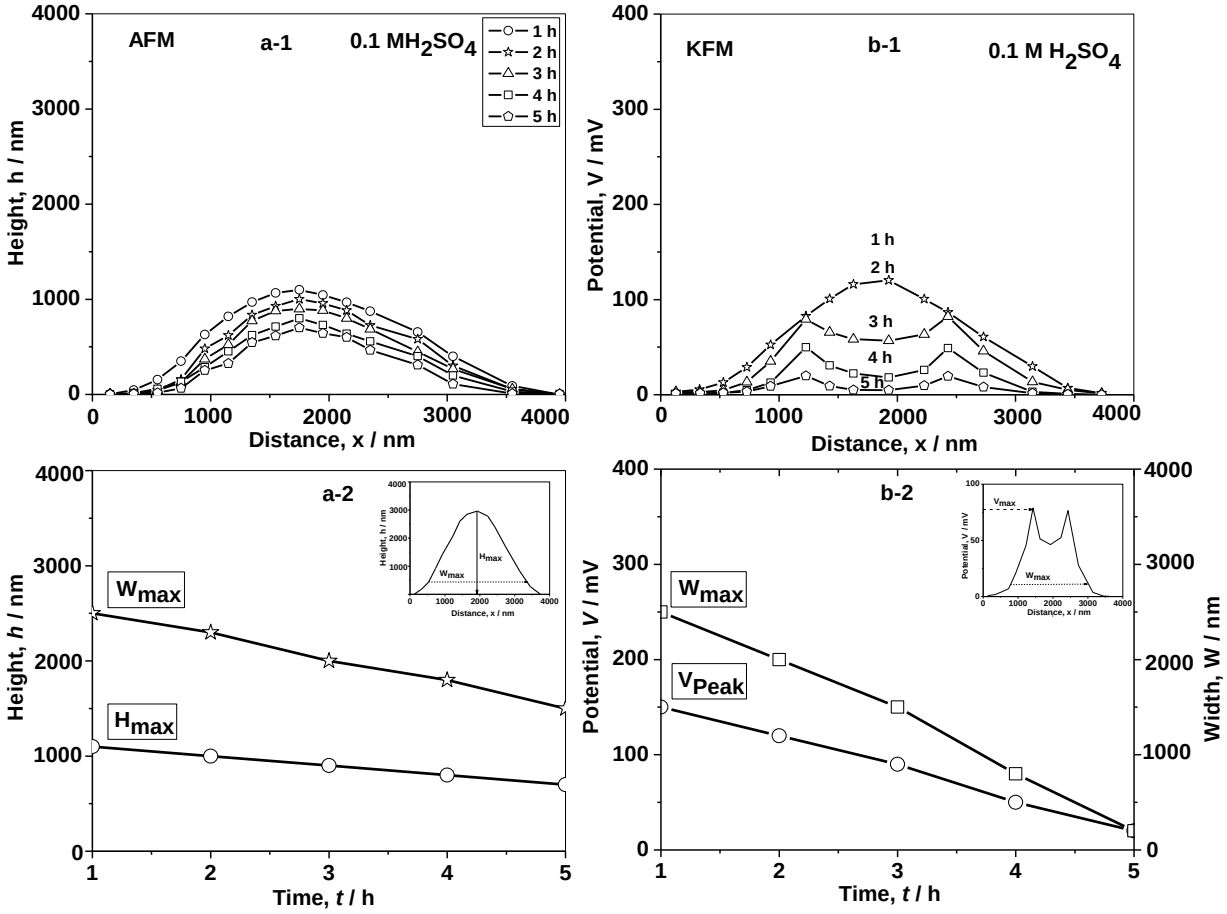

Figure 3. Line profiles of AFM and KFM images of iron nanoparticle in 0.1M H_2SO_4 at different hours, (a-2) The maximum height (H_{max}) and (b-2) the peak potential (V_{peak})

Figure 2 shows the surface topography (AFM) and the potential distribution (KFM) on the iron nanoparticle in 0.1 M H_2SO_4 for different hours. Pure iron nanoparticles were immerged in an acid at different time and were imaged by AFM and KFM. The iron nanoparticles were imaged by AFM and KFM on freshly cleaned Pt substrates. In AFM, the mapping of the nanoparticle produces global shape, then, its size is reduced slightly with increase in processing time in acidic solution. The height of the nanoparticle decreases from 1200 nm at 1 h to 800 nm at 5 h. On the other hand, the corresponding KFM image which shows the change of potential value of nanoparticle is drastically reduced. The shape of the nanoparticles varied from image to image. Actually, the maximum surface potential decreases from 150 mV at 1 h to 20 mV at 5 h. This is due to the rapid corrosion rate of pure iron nanoparticle in an acidic solution. Although the KFM image after 2 h shows the global shape, however, it becomes the corrupted image after 3 h due to the corrosion of nanoparticles. In this way, the steep decrease in the surface potential was indicated by highly corrosion rate of iron in 0.1 M H_2SO_4.

Figure 3 shows the line profile of AFM (a-1) and KFM (b-1) for the iron nanoparticle in an acidic solution. These line profiles produce the peak and the shape of the mountain in each mapping of

AFM and KFM at the first time. The peak of the curve in AFM slightly decreases with increase in time. On the other hand, its corresponding potential peak in KFM is drastically reduced with time. The change of the peak can be noticeable due to the corrosion of the nanoparticles. The maximum height (H_{max}) and width (W_{max}) of the AFM line profile are shown in a-2, and the corresponding potential peak (V_{peak}) of the KFM is shown in b-2. In a-2, W_{max} and H_{max} in AFM change slowly as a test time. On the other hand, the peak potential (V_{max}) in KFM decreases severely with increase in time. It is found that the corrosion of pure Fe takes place very heavily, which is shown in KFM strongly.

3.2. Effect of concentration of H_2SO_4 on pure iron nanoparticles:

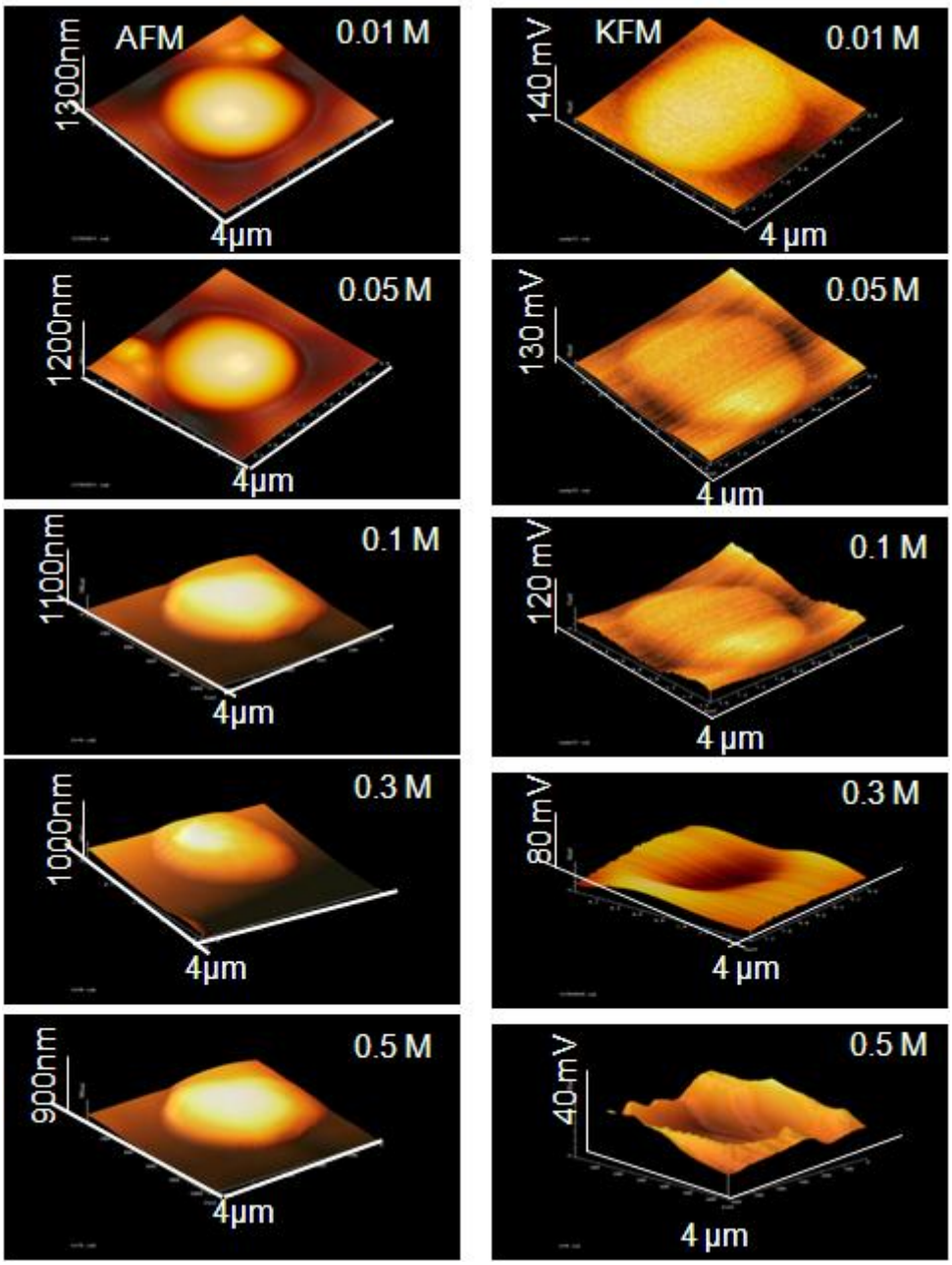

Figure 4. AFM (left) and KFM (right) images of pure iron nanoparticle in different concentration of H_2SO_4.

Figure 4 depicts the surface topography (AFM) and potential distribution (KFM) of pure Fe nanoparticle in different concentration of H_2SO_4. The hight of the nanoparticle slightly decreases from 1300 nm at 0.01 M to 900 nm at 0.5 M H_2SO_4. On the other hand, the maximum potential decreases from 140 mV at 0.5 M to 40 mV at 0.5 M H_2SO_4. Thus the effect of acid on surface potential (KFM) is high when the acid concentration is increased. The increase in the concentration of the acid increases the corrosion of the pure Fe nanoparticle, indicated by the decrease in the surface potential [18]. The shape of KFM for the nanoparticles is varied with increase in the concentration of the acid that resulted. Although the KFM image in 0.05 M shows the global shape, however, it becomes the corrupted image in 0.3 M H_2SO_4 due to the corrosion of nanoparticles. This is due to the corrosion of pure Fe nanoparticle in the high concentration of acidic solution. The steep decrease in the surface potential was indicated by high corrosion rate of iron in the high concentration of the acid [19].

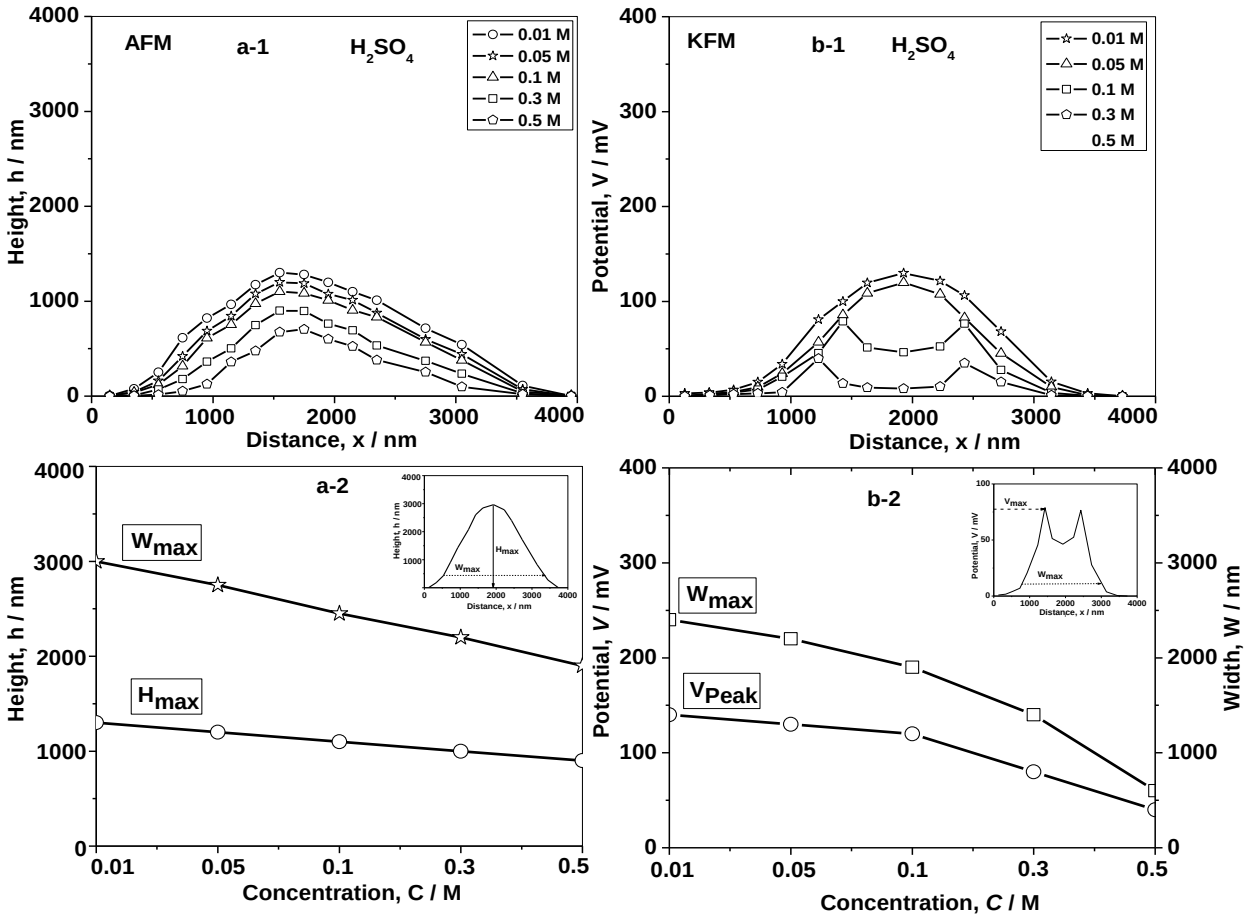

Figure 5. Line profiles of AFM and KFM images of iron nanoparticle in different concentration of H_2SO_4, (a-2) the maximum height (H_{max}) and (b-2) the peak potential (V_{peak}).

Figures 5(a-1) and (b-1) show the line profile of AFM and KFM respectively in different concentration of acid. The corresponding maximum height (H_{max}) of AFM and the peak potential (V_{peak}) of KFM for the nanoparticle are shown in the figure 5 (a-2) and (b-2). The size as well as the surface potential of the nanoparticle decreases with increase in the concentration of the acid. The change of shape of KFM in 0.1 M acid is highly noticeable, which is thought due to the corrosion of

the nanoparticles. This is because that the acid solution at 0.1 M destroys the passive film of the Fe nanoparticle. Thus in KFM, V_{peak} is strongly reduced from the concentration of 0.1 M in an acidic solution. Moreover, it is found that KFM is more sensitive to the electrochemical reaction of nanoparticle as compared to AFM.

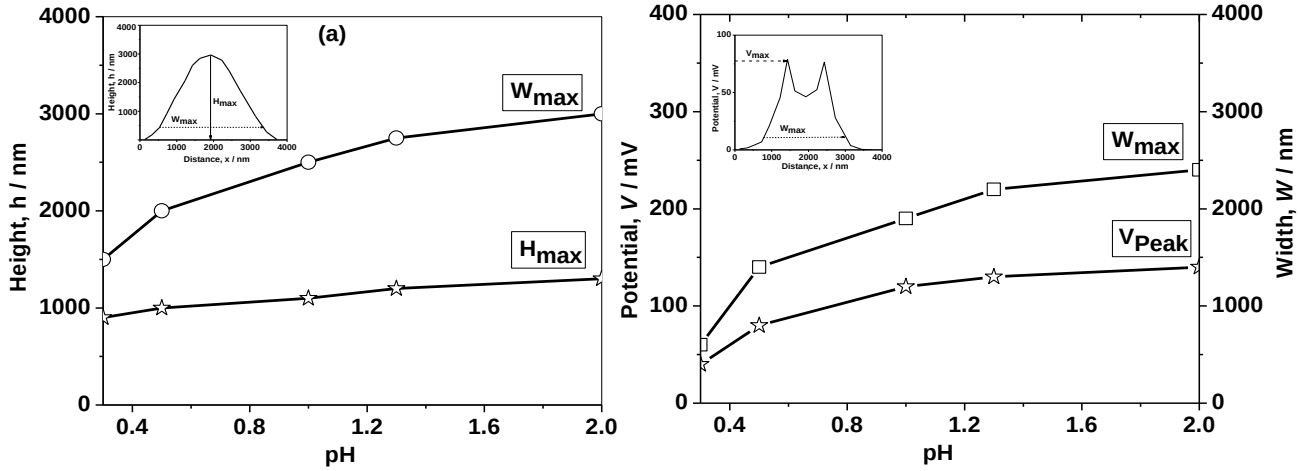

Figure 6. (a) The maximum height (H_{max}) and (b) the peak potential (V_{peak}) of pure iron nanoparticle with respect to pH of the solution from line-scan analysis.

Figure 6 (a) and (b) represent the maximum height (H_{max}) in AFM and the peak potential (V_{peak}) in KFM for pure iron nanoparticle with respect to pH of the solution. The H_{max} of AFM for the nanoparticle is found to be constant between 900 – 1300 nm. On the other hand, the V_{peak} in KFM of the nanoparticle strongly increases from 40 mV at pH 0.3 to 140 mV at pH 2.0. Thus the surface potential of the nanoparticle of KFM increases with increase in the pH of the solution. This clearly indicates that the surface potential by KFM for the nanoparticle strongly corresponds to the corrosion of the nanoparticle. It was elucidated that the pH of the solution affected the corrosion behavior of the nanoparticles and the KFM image was strongly changed corresponding to the electrochemical reactions of the nanoparticle in acidic solution.

3.3. Effect of treatment period on SUS steel nanoparticles in 0.1 M H_2SO_4:

Figure 7 shows the shape in AFM and potential distribution in KFM for SUS steel nanoparticle in 0.1 M H_2SO_4 for different hours. In AFM, the mapping of the nanoparticle produces a global shape, and it keeps the same shape after 5 hours. In KFM, the top potential decreases a little from 150 mV at 1 h to 110 mV at 5 h. As compared to Fig.2, the surface potential of SUS nanoparticle is 90 mV higher than that of pure Fe nanoparticle after 5 h. This result is thought to show the higher corrosion resistance of SUS nanoparticle in an acidic solution due to keeping passive film [20].

Figures 8 (a-1) and (b-1) represent the line profile of AFM and KFM images of SUS steel nanoparticle in 0.1 M H_2SO_4 at different hours.

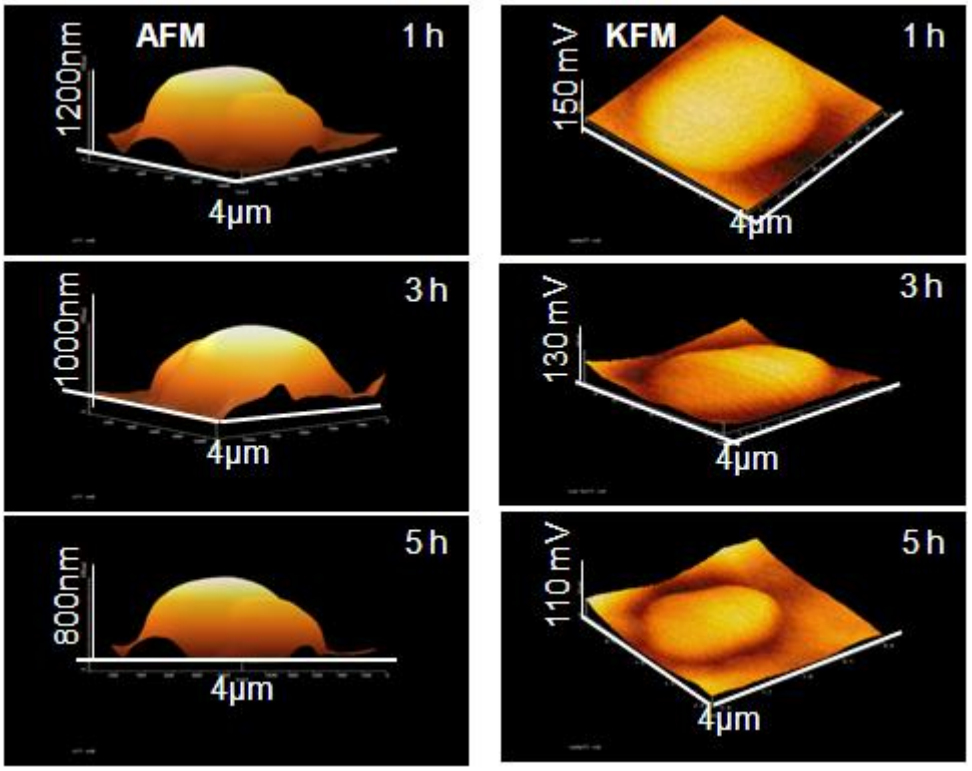

Figure 7. AFM (left) and KFM (right) images of SUS nanoparticle in 0.1M H_2 SO_4 at different hours.

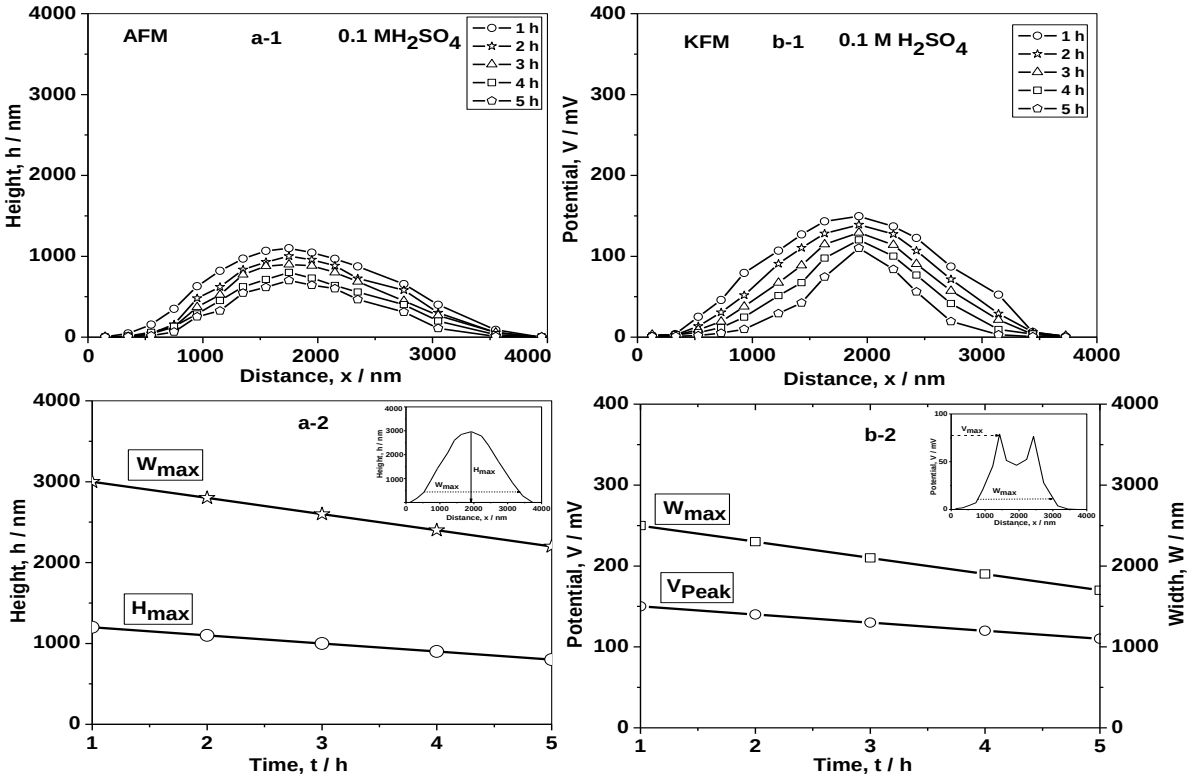

Figure 8. Line profiles of AFM and KFM images of SUS nanoparticle in H_2SO_4 at different hours, (a-2) the maximum height (H_{max}) and (b-2) the peak potential (V_{peak})

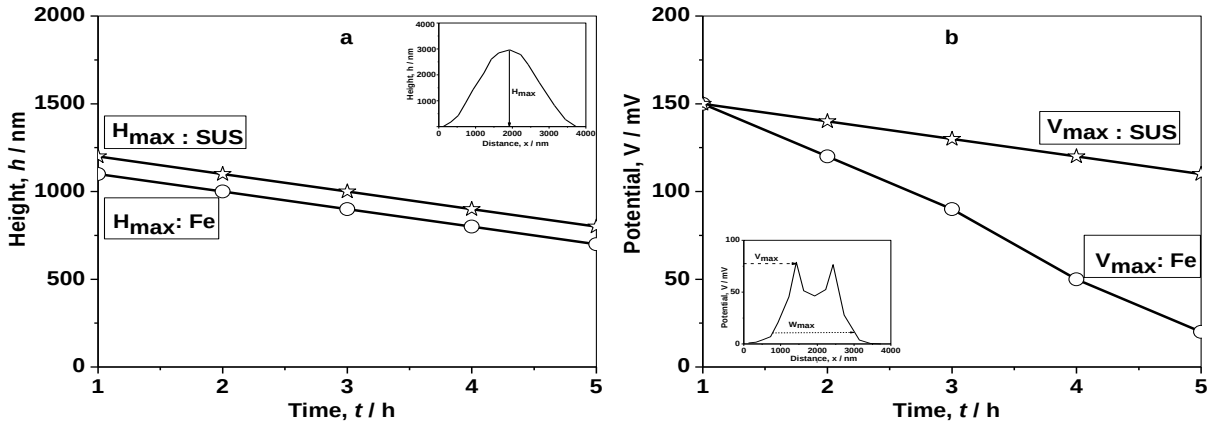

Figure 9. Comparison of AFM and KFM images of iron and SUS nanoparticle in H_2SO_4 at different hours, (a) the maximum height (H_{max}) and (b) the peak potential (V_{peak})

The corresponding maximum height (H_{max}) of AFM and the peak potential (V_{peak}) of KFM for the SUS nanoparticle are shown in the figure 8 (a-2) and (b-2). The surface potential and the size of the stainless steel nanoparticle decrease very slowly with increase in time in an acidic solution. This is because that the SUS nanoparticle possesses higher corrosion resistance in an acidic solution. As compared to Figure 3, the decrease in size as well as its surface potential of the SUS nanoparticle is very less compared to the pure iron nanoparticle. This is due to the formation of passive film on SUS nanoparticle that protects the nanoparticle from being corroded. Therefore, it can be indicated that the corrosion hardly takes place at the SUS nanoparticle in acidic solution.

Fig.9 shows the comparison of AFM and KFM images of iron and SUS nanoparticle in H_2SO_4 at different hours, by (a) the maximum height (H_{max}) and (b) the peak potential (V_{peak}). In AFM, H_{max} of iron and SUS nanoparticle are almost the same level. However, in KFM, the decrease of the surface potential of pure Fe nanoparticle is much sharper than SUS nanoparticle. This was due to the higher corrosion resistance of SUS nanoparticle in an acidic solution. Therefore, the corrosion of SUS nanoparticle was thought suppressed by the formation of protective film on the surface. It was concluded that SUS nanoparticle exhibited excellent corrosion resistance compared to pure Fe in 0.1 M H_2SO_4 by the formation of protective film on the surface.

4. CONCLUSION

The topographies and the surface potentials on nanoparticles were simultaneously measured by using AFM and KFM. Specially, KFM offered attractive information by obtaining high-resolution maps of the surface potential distribution on nanoparticles which investigated the corrosion processes occurring at the surface. The study on the effect of concentration of H_2SO_4 at different duration provides an estimate of corrosion of nanoparticles.

The correlation between the surface potential of the nanoparticle and corrosion behaviour was investigated by AFM and KFM in 0.1 M H_2SO_4 with different time. The size and the surface shape of

pure Fe nanoparticles decreased with time in an acidic solution, indicating the corrosion of nanoparticles. Similarly, the surface potential of pure Fe nanoparticles by KFM decreased with increase in the concentration of the acidic solution. On the other hand, there was no significant change in the surface potential of SUS nanoparticles with increase in the time in an acidic solution. The decrease in surface potential of the SUS nanoparticle was very slow compared to pure Fe nanoparticle. This was due to the formation of passive film on the surface of SUS nanoparticle. It was concluded that compared to pure Fe nanoparticle, SUS nanoparticle exhibited excellent corrosion resistance in 0.1 M H_2SO_4.

References

1. R.M. Crooks, M. Zhao, L. Sun, L. Chechik and L.K. Yeung, *Acc. Chem. Res.*,34 (2000) 181 -190
2. O.V. Salata, *J. Nanobiotechnology,* (2004), 1 -6
3. C.J. Murphy, *Science,* 298 (2002) 2139 – 2141
4. K. Fukushima and I. Yamada, *J. Appl. Phys.,* 65 (1989) 619-623
5. H.Y Ha, S.W. Nam, T.H. Lim, I.H. Oh and S.A. Hong, *J. Membr. Sci*., 111 (1996) 81- 92
6. M.R. Hoffman, S.T. Martin, W. Choi, and D.W. Bahenman, *Chem Rev.,* 95 (1995) 69- 96
7. Roohangiz Zandi Zand, Kim Verbeken and Annemie Adriaens, *Int. J. Electrochem. Sci.,* 8 (2013) 4924 – 4940
8. Cheng-Kuo Lee, *Int. J. Electrochem. Sci*., 7 (2012) 12941 - 12954
9. S. Sadewasser, Th.; Glatzel, S. Schuler, S. Nishiwaki and Ch. M. Lux-Steiner, *Thin Solid Films,* 257 (2003) 431–432
10. H. Hoppe, T. Glatzel, M. Niggemann, A. Hinsch, M.C. Lux-Steiner and N.S. Sariciftci, *Nano Lett*., 5 (2005) 269-274
11. T. Hallam, C.M. Duffy, T. Minakata, M. Ando and H. A. Sirringhaus, *Nanotechnology,* 20 (2009) 025203
12. L.M. Liu and G.Y. Li, *Appl. Phys. Lett*., 96 (2010) 083302
13. M. Stratmann, *Corros. Sci.,* 27 (1987) 869–72
14. S. Yee, R.A. Oriani, M. Stratmann, *J. Electrochem. Soc.,* 138 (1991) 55-61
15. O. Albani, S.M. Huang and R.A. Oriani, *Corrosion* 50 (1994) 331–333
16. M. Stratmann, H. Streckel, K.T. Kim and S. Crockett, *Corros. Sci*., 30 (1990) 715–734
17. R.T. Atanasoski, S.M. Huang, O. Albani and R.A. Oriani, *Corros. Sci*., 36 (1994) 1513–1521
18. M. Behzadnasab, S.M. Mirabedini, K. Kabiri and S. Jamali, *Corros. Sci.,* 53 (2011) 89-98
19. A M. Atta, OE. El-Azabawy, H.S. Ismail and M.A. Hegazy, *Corros. Sci.,* 53 (2011) 1680-1689.
20. Eleonora Bettini, Ulf Kivisäkk, Christofer Leygraf and Jinshan Pan, *Int. J. Electrochem. Sci.,* 9 (2014) 61 - 80